Modelling non-ductile reinforced concrete columns

Anita Amirsardari[1*], Pathmanathan Rajeev[2], Helen M. Goldsworthy[3*], Elisa Lumantarna[4*]

1. Corresponding Author. PhD Candidate, Department of Infrastructure Engineering, University of Melbourne, Parkville, 3010, Australia. Email: amia@student.unimelb.edu.au
2. Senior Lecturer, Department of Civil and Construction Engineering, Swinburne University of Technology, Hawthorn, 3122, Australia. Email: prajeev@swin.edu.au
3. Associate Professor, Department of Infrastructure Engineering, University of Melbourne, Parkville, 3010, Australia. Email: helenmg@unimelb.edu.au
4. Lecturer, Department of Infrastructure Engineering, University of Melbourne, Parkville, 3010, Australia. Email: elu@unimelb.edu.au

* Bushfire and Natural Hazards Cooperative Research Centre

ABSTRACT:

The aim of this study was to model the cyclic response of non-ductile reinforced concrete columns with increasing drift levels until the columns experience a loss of axial load carrying capacity. The adopted modelling approach is intended to be used for the global seismic analysis and assessment of gravity reinforced concrete moment resisting frames, therefore, the adopted method needs to be both efficient and accurate. The effect of incorporating various inelastic mechanisms typical of non-ductile columns was investigated, including flexural and shear behaviour and bond-slip of longitudinal reinforcing bars. Simulated column response under cyclic lateral loading is compared with experimental results available in the literature. The results demonstrate the importance of incorporating the shear behaviour of the columns, as significant strength and stiffness degradation often occurs after the yield moment of the columns is reached.

Keywords: Non-ductile reinforced concrete, columns, bond-slip, shear failure, axial load failure

1 INTRODUCTION

To assess the performance of buildings it is necessary to accurately model the various component mechanisms since collapse of buildings is initiated by component failures. This study looks at the various modelling techniques to simulate non-ductile column response to cyclic loading with a particular focus on the shear response of columns. The modelling techniques are to be used in OpenSees (McKenna et al., 2000), a macro finite element space, to conduct assessment of non-ductile gravity or secondary moment resisting frames; therefore the adopted approach needs to be both efficient and reliable. Furthermore, since the objective is to assess the performance of gravity frames, the drift capacity of the columns at lateral load failure and axial load failure are of interest.

Many frames in Australia, whether they form part of the primary or secondary system, are designed as ordinary moment resisting frames (OMRFs). This means that they have non-ductile detailing and are vulnerable to sudden undesirable failure mechanisms. The detailing deficiencies which have been identified to be typical of non-ductile columns include (Elwood & Moehle, 2003; Fardipour, 2012, Wilson et al., 2015):

- Ties are spaced widely and poorly configured
- Splices located in potential hinge regions and have insufficient lap lengths
- Columns are highly loaded under gravity loading

These detailing deficiencies make the columns vulnerable to flexural (F), flexure-shear (FS), shear (S) and bond failures. A brief description of the various failure mechanisms is provided below:

- **Flexure dominated columns** are described as columns which reach their ultimate bending capacity, and failure is initiated due to spalling of cover concrete followed by buckling or fracture of longitudinal bars.
- **Flexure-shear dominated columns** are characterised as columns which initially experience flexural yielding, but with deterioration of the plastic hinge region, critical shear cracks are formed. The loss of axial load capacity of the column is due to sliding of the column along the critical shear crack as the frictional resistance reduces.
- **Shear governed columns** are described as columns which experience lateral strength degradation prior to yielding of longitudinal bars. Failure occurs due to sudden propagation of one or more critical cracks (tensile failure), or crushing of concrete (compressive failure).
- **Bond failure** is associated with bar-slip of the longitudinal bars at the ends of the column resulting in rigid body rotations which can significantly increase the column flexibility; however ultimate failure of the column is often associated with another mechanism: flexure, flexure-shear, or shear failure.

Current methods of assessment (NSZEE, 2006; Stirrat et al., 2014) involve determining the expected failure mechanisms which are likely to govern the response in order to determine the drift capacity of the column at (i) ultimate conditions or initiation of lateral strength degradation, $\frac{\Delta_u}{L}$ and $\frac{\Delta_s}{L}$ respectively, and (ii) axial load failure, $\frac{\Delta_a}{L}$. In reality, column failure is often due to a combination of failure mechanisms. For the purpose of assessment, if multiple failure mechanisms are expected, the drift capacity of the lower one should be taken. Past studies have often assumed that the critical failure modes of non-ductile columns are S and FS, and therefore ignore the flexural failure modes (Elwood & Moehle, 2003; Jeon et al., 2015, LeBorgne & Ghannoum, 2014a).

2 MODELLING COLUMN RESPONSE MECHANISMS

The lateral deformation experienced by RC columns subjected to lateral loading is predominantly due to flexural, slip, and shear deformations, as illustrated in Figure 1. Thus, to model the seismic response of columns, each deformation component needs to be simulated. The following sub-sections describe best practice for modelling the various response and failure mechanisms of columns.

2.1 FLEXURAL RESPONSE

Generally, the flexural response of columns can be accurately simulated with distributed plasticity elements. The element response is determined by a weighted integration of the fibre-section response at each integration point, hence allowing non-linear behaviour to be modelled along the length of the member.

The fibre sections are modelled with non-linear uniaxial material models which define the longitudinal reinforcement and concrete material properties, shown in Figure 2. Often the core and cover concrete are modelled separately to account for the confinement effect, although for non-ductile columns the confinement factor is very small. Furthermore, for global analysis of RC structures it is often assumed that the behaviour of the reinforcement is the same in tension and compression. In reality the stress-strain relationship of the reinforcement is different in tension and compression due to the Bauschinger effect and buckling. However, there is still insufficient understanding about buckling and a consensus does not exist about the most suitable method to model the behaviour. Nevertheless, numerous studies exist in which analytical models have been proposed based on experimental testing (Dhakal & Maekawa, 2002; Gomes & Appleton, 1997).

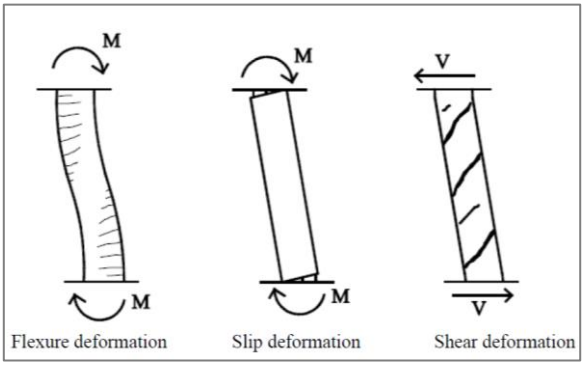

Figure 1: The lateral deformation components of RC column (Lodhi, 2010)

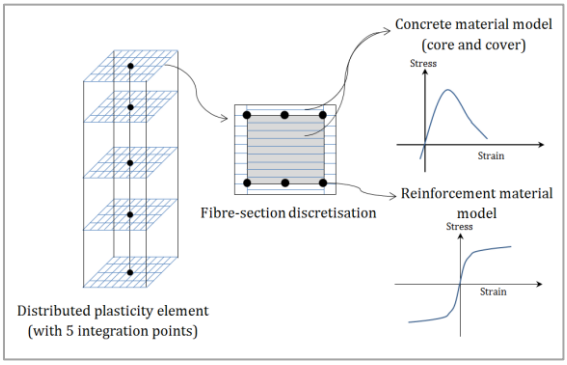

Figure 2: Distributed plasticity element modelled with fiber sections

2.2 BAR-SLIP

Bar-slip causes rigid body rotations which can significantly increase the column flexibility. It can be incorporated in an FE model via a zero-length spring; however recent studies recommend incorporating bar-slip with zero-length fibre sections (Berry, 2006; Ghannoum & Moehle, 2012; Zhao & Sritharan, 2007). The section has the same geometry as the actual column section; but the material properties for the concrete and steel fibres are altered. The critical strain values which define the concrete and steel model are amplified by a factor which is dependent on the amount of slip expected. The use zero-length fiber-section to model bond-slip is preferred over zero-length springs because fiber models allow the adjustment of the neutral axis location based on the applied axial load and loading direction and thus provide more accurate results (Ghannoum & Moehle, 2012).

2.3 SHEAR RESPONSE

As discussed previously, the shear response of a non-ductile column is often expected to be a key contributor to the critical failure mechanism. Currently the parameters required to model the shear response of columns are approximated by empirical equations and at this stage there is no consensus on the best available model.

Shear response is added to columns via zero length spring elements. A key advancement in uniaxial materials models that define the shear response was a model developed by Elwood (2004) which is implemented in OpenSees and known as the *limit state material* model. Unlike prior material models, which were only capable of capturing shear failure if the shear strength was less than the flexural strength of the column (see Figure 3), the *limit state material* model is capable of detecting shear failure due to exceedance of shear capacity, or exceedance of shear drift capacity, shown in Figure 4. Hence the model captures shear failure which occurs after flexural yielding as a result of the shear capacity of the column decreasing with increased inelastic deformations. Once the shear strength or deformation capacity is exceeded, the shear spring backbone is redefined to include the user-defined degrading shear slope, K_{deg}, and residual force, F_{res}. Due to the series nature of the elements K_{deg} may be calculated using:

$$K_{deg} = \left(\frac{1}{K_{deg}^{t}} - \frac{1}{K_{unload}}\right)^{-1} \quad (1)$$

Where: K_{deg}^{t} is the total degrading stiffness

$K_{deg}^{t} = \frac{V_u}{(\Delta_a - \Delta_s)}$ where V_u peak shear strength, Δ_s and Δ_a are the displacements at shear and axial load failure respectively.

K_{unload} is the flexural degrading stiffness

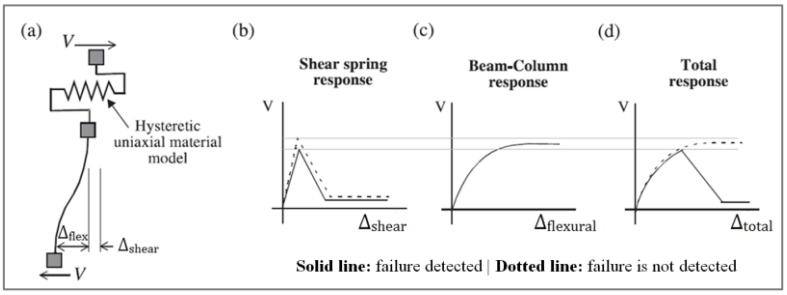

Figure 3: Material model capturing shear failure for columns with shear strength less than the flexural strength, adapted from Elwood (2004).

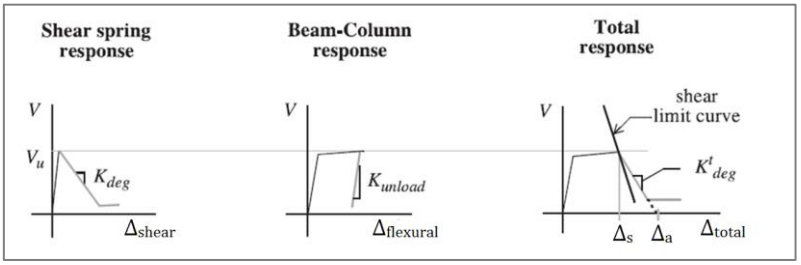

Figure 4: Material model capturing shear failure due to exceedance of shear displacement capacity, adapted from Elwood, (2004)

While the *limit state material* model has been shown to satisfactorily model the behaviour of columns failing in shear, there are some limitations to the model. Elwood (2004) explains that

convergence issues may occur if the beam-column experiences flexural degradation prior to shear failure since multiple solutions are possible. LeBorgne (2012) built on the work conducted by Elwood (2004) and introduced a new uniaxial material, called the *pinching limit state material*, which is also implemented in OpenSees. The *pinching limit state material* has overcome some of the limitations of the *limit state material.*

3 METHODOLOGY

The element configuration as presented in LeBorgne (2012) and Ghannoum and Moehle (2012) for the incorporation of flexural, bar-slip and shear response is adopted in this study and is illustrated in Figure 5. The plastic hinge length, which is assumed to be equal to the depth of the column (D_c), is modelled with a forced-based distributed plasticity element with two integration points, and the remaining portion of the column (i.e. L-2D_c, where L is the length of the column) is modelled with a forced-based distributed plasticity element with four integration points. It is noted that the shear spring is modelled with the *pinching limit state material* instead of the *limit state material* as it appears to have fewer convergence issues when the beam-column element experiences flexural degradation prior to shear failure. The details of the selected uniaxial material models for flexural response and empirical equations for shear response are discussed in the following sub-sections.

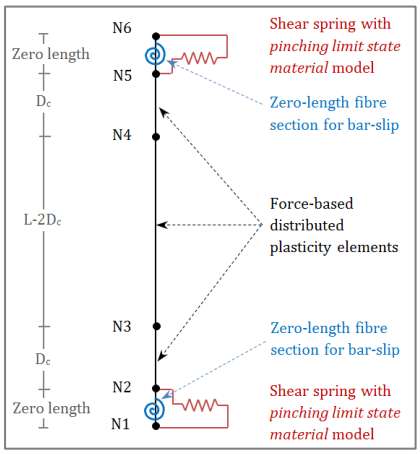

Figure 5: Modelling technique adopted in this study

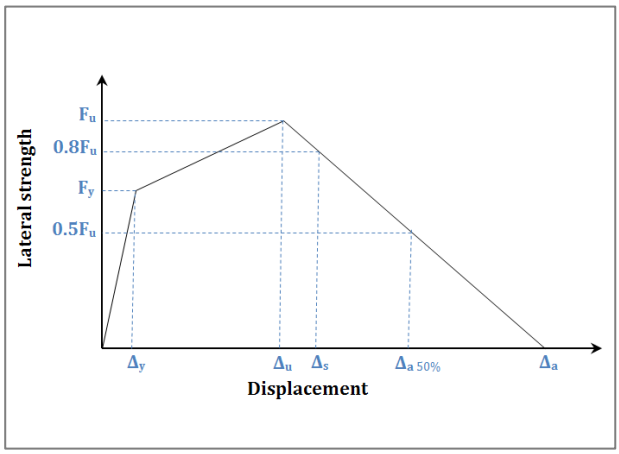

Figure 6: Definition of critical points for the lateral strength-displacement response of non-ductile columns

3.1 UNIAXIAL MATERIAL MODELS

The concrete behaviour is modelled using *Concrete04*, a uniaxial concrete stress-strain material model developed by Popovics (1973), which is available in OpenSees. The effect of confinement is accounted for by using a model developed by Mander, Priestley, and Park (1988). For computational efficiency and numerical stability the Bauschinger effect is not included in the model, and the steel is modelled using *Steel02*, the Giuffré-Menegotto-Pinto model (Menegotto & Pinto, 1973). However, the strains in the plastic hinge region are monitored to determine if buckling of bars is expected in accordance with the buckling strain limit suggested by Moyer and Kowalsky (2003):

$$\varepsilon_{sb} = 3\left(\frac{Ks}{d_b}\right)^{-2.5} \quad (2)$$

Where: s is the spacing of the ties
d_b is the diameter of longitudinal bars
K is the effective length factor which may be taken as 1.0

3.2 EMPIRICAL MODELS FOR SHEAR RESPONSE

In order to determine suitable empirical equations to define deformation limits, and hence the shear spring response for FS columns, three well established models available in the literature for non-ductile columns were examined:

- Model 1: Elwood and Moehle (2003)
- Model 2: LeBorgne (2012), LeBorgne and Ghannoum (2014)
- Model 3: Wibowo et al. (2014), Wilson et al., (2015)

A summary of the database for the three models is provided in Table 1. The definition of the critical points associated with the column response varies from one model to the next. The points chosen as critical points in this study are shown in Figure 6, and where possible the critical points defined in the three models are also illustrated. The equations proposed by each model are provided in Table A1 in the Appendix.

Table 1: Summary of empirical based models

Database and Model Detail	**Model 1**	**Model 2**	**Model 3**
Number of specimens	50 columns for determining Δ_s, and 12 columns for determining Δ_a	32 columns	46 columns
Method used to determine proposed equations	Δ_s is based on curve fitting with experimental data. Δ_a is based on the classical shear-friction mechanism and the effective coefficient of friction is based on experimental tests.	Proposed equations are based on regression analysis.	Δ_u determined based on yield and plastic curvatures. Δ_a is determined based on curve fitting with experimental data. Δ_s is determined by linear interpolation between Δ_u and Δ_a.
Range of parameters in database			
Concrete compressive strength	$13.1 \leq f_c' \leq 44.8$ *MPa*	$19.3 \leq f_c' \leq 46.9$ *MPa*	*NA*
Longitudinal reinforcement yield stress	$324.1 \leq f_{yl} \leq 542.0$ *MPa*	$330.7 \leq f_{yl} \leq 523.6$ *MPa*	*NA*
Longitudinal reinforcement ratio	$0.01 \leq \rho_l \leq 0.04$	$0.01 \lesssim \rho_l \lesssim 0.04$	$\rho_l \leq 0.02$
Shear span to depth ratio	$2.0 \leq \frac{a}{d} \leq 4.0$	$1.5 \lesssim \frac{a}{d} \lesssim 4.0$	$1.0 \leq \frac{a}{d} \leq 5.5$
Transverse reinforcement spacing to depth ratio	$0.2 \leq s/d \leq 1.2$	$0.1 \lesssim s/d \lesssim 1.2$	*NA*
Transverse reinforcement yield stress	$317.2 \leq f_{yt} \leq$*648.1 MPa*	$316.9 \leq f_{yt} \leq$ *565.0 MPa*	*NA*
Transverse reinforcement ratio	$0.0010 \leq \rho_t \leq 0.0065$	$0.0010 \lesssim \rho_t \lesssim 0.014$	$\rho_t \leq 0.004$
Maximum shear stress	$0.23 \leq \frac{v}{\sqrt{f_c'\ (MPa)}} \leq 0.71$	*NA*	*NA*
Axial load ratio	$0.0 \leq \frac{P}{A_g f_c'} \leq 0.6$	$0.0 \leq \frac{P}{A_g f_c'} \leq 0.6$	$0.0 \leq \frac{P}{A_g f_c'} \leq 0.65$

NA: not available

Deformation at shear failure (Δ_s) in Models 1 and 3 is defined as the displacement at which the shear resistance drops below 80% of the maximum shear recorded; this is the conventional method of defining lateral strength failure. In Model 2, the deformation limit at shear failure is determined based on the total rotation limit (θ_f) allowed in the plastic hinge region, and it corresponds to the deformation at which the maximum shear force was recorded (referred to as the ultimate displacement in this study, Δ_u). The deformation limit at axial failure (Δ_a) in Model 1 is defined as the displacement at which axial load failure was observed in the experiment; this approximately corresponds to the displacement at which the shear resistance dropped to zero. The deformation limit at axial failure in Model 2 is not directly provided; rather the shear displacement corresponding to the difference between the displacement at which ultimate shear force and residual lateral strength was observed in the

experiment is provided (Δ_r). The deformation limit at axial failure in Model 3 refers to the displacement at which the shear resistance drops below 50% of the maximum applied shear force ($\Delta_{a\ 50\%}$).

A database of 20 columns (details provided in Table A2), for which experimental results are available in the literature, was compiled in order to compare the critical experimental parameters with parameters calculated using the empirically based models. The columns included in the database are representative of existing RC columns in Australia. The purpose of comparing the models with a database compiled by the authors was to reduce bias and to examine the applicability of the models. Furthermore, as noted previously, the critical parameters in each model are in various forms and not directly comparable. Hence, suitable calculations are performed to change the parameters so that they are directly comparable:

- Plastic hinge rotation limit (θ_f) in Model 2 was changed to inter-storey drift limit using:

$$\frac{\Delta_u}{H} = \frac{\phi_y\left(\frac{h_i^2}{2}\right)\left(1-\frac{h_i}{3H}\right)+\theta_p h_i}{H} \quad (3)$$

Where: h_i is the height at which drift is calculated, i.e. the shear span of the column
H is the shear span of the column
ϕ_y is the yield curvature obtained from sectional analysis
θ_p is the plastic rotation, $\theta_p = \theta_f - \theta_y$
Where: θ_f is the total plastic hinge rotation provided by Model 2
θ_y is the yield rotation
$\theta_y = \phi_y L_p - \frac{\phi_y L_p^2}{2H}$, where L_p is the plastic hinge length

- The axial drift limit in Model 3 ($\Delta_{a\ 50\%}$/L) was extended using linear interpolation to the point at which the shear capacity had dropped to zero (referred to as Δ_a /L) so that it was easily comparable with Model 1 and experimental data.
- It was not possible to change Δ_r of Model 2 to Δ_a, thus the drift at axial failure of Model 2 cannot be directly compared with the other models.

A summary of the predicted and experimental drift ratios is provided in Table 2. The drift at shear failure for Model 1 and 3, and the ultimate drift for Model 2, are compared with experimental drift at ultimate strength in Figure 7. The experimental drift at 80 % of the peak strength was not compared since this was not provided in all of the studies. Note that it is expected that Model 1 and Model 3 will overestimate the drift in comparison with the experimental result, since the predicted drift at shear failure for these models is at 80 % of peak strength rather than at ultimate drift. However, this is not observed for Model 3 which actually tends to under-estimate the drift.

The drifts at axial load failure (Δ_a /L) for Model 1 and 3 are compared with experimental drifts at axial load failure in Figure 8. Model 1 clearly provides a very good match with experimental results, whereas Model 3 tends to overestimate the drift. It is important to note that Model 3's overestimation in the context of this study may be due to the adoption here of Δ_a /L as the drift at axial load failure rather than $\Delta_{a\ 50\%}$/L which was used by (Wibowo et al, 2014) when comparing their model to experimental results. Also it is observed that Model 3 does not match well with the experimental results at very low axial loads, see Table 2 for drift predictions Saatcioglu and Ozcebe (1989) U1 column which was not included in Figures 7

and 8. It is not possible to directly compare Model 2 with experimental results in Figure 8**;** however, based on the results shown in Table 2, it can be seen that the prediction for Δ_r tends to be significantly higher than Δ_a for some columns, suggesting that the model significantly over-predicts the drifts at axial load failure. Based on the comparison made with the experimental results compiled in this study, Model 1 tends to provide the best estimate of the critical parameters. Therefore Model 1 is adopted in this study to define the shear spring response.

Table 2: Experimental and calculated drift ratios using the three models

Specimen	Experiment		Model 1		Model 2			Model 3		
	Δ_u/L	Δ_a/L	Δ_s/L	Δ_a/L	Δ_s/L	$\Delta_{a\,50\%}/L$	Δ_a/L	θ_f	Δ_u/L	Δ_r/L
Sezen (2002) Spec 1	0.019	0.050	0.025	0.055	0.016	0.034	0.060	0.014	0.015	0.237
Sezen (2002) Spec 2	0.009	0.019	0.013	0.022	0.011	0.018	0.032	0.006	0.006	0.237
Sezen (2002) Spec 3	0.009	0.029	0.013	0.022	0.011	0.018	0.032	0.006	0.006	0.237
Sezen (2002) Spec 4	0.021	0.055	0.025	0.055	0.016	0.034	0.060	0.014	0.015	0.237
Lynn et al. (1996) 3CLH18	0.010	0.021	0.025	0.031	0.018	0.034	0.064	0.012	0.013	0.270
Lynn et al. (1996) 2CLH18	0.026	0.031	0.026	0.031	0.018	0.046	0.088	0.013	0.014	0.224
Lynn et al. (1996) 3SLH18	0.010	0.036	0.025	0.031	0.018	0.034	0.064	0.012	0.013	0.270
Lynn et al. (1996) 2SLH18	0.021	0.036	0.026	0.031	0.018	0.046	0.088	0.013	0.014	0.224
Lynn et al. (1996) 2CMH18	0.010	0.010	0.019	0.013	0.009	0.013	0.019	0.006	0.006	0.230
Lynn et al. (1996) 3CMH18	0.010	0.021	0.019	0.013	0.009	0.013	0.021	0.007	0.007	0.268
Lynn et al. (1996) 3CMD12	0.016	0.023	0.022	0.031	0.013	0.023	0.040	0.010	0.011	0.247
Lynn et al. (1996) 3SMD12	0.016	0.021	0.021	0.031	0.012	0.021	0.037	0.010	0.010	0.255
Ho and Pam (2004) 1A	0.018	0.050	0.030	0.022	0.023	0.047	0.086	0.017	0.020	0.215
Ho and Pam (2004) 2A	0.014	0.025	0.027	0.015	0.016	0.028	0.047	0.013	0.016	0.174
Fardipour (2012) Spec 1	0.017	0.050	0.023	0.021	0.020	0.035	0.062	0.009	0.011	0.046
Fardipour (2012) Spec 2	0.017	0.025	0.022	0.021	0.017	0.027	0.045	0.009	0.011	0.021
Fardipour (2012) Spec 3	0.011	0.015	0.016	0.013	0.007	0.010	0.015	0.006	0.008	0.005
Fardipour (2012) Spec 4	0.010	0.015	0.017	0.010	0.006	0.010	0.016	0.006	0.008	0.069
Saatcioglu and Ozcebe (1989) U1	0.046	0.085	0.033	0.100	4.29	10.71	21.42	0.022	0.022	0.217
Saatcioglu and Ozcebe (1989) U2	0.032	0.057	0.026	0.055	0.020	0.038	0.068	0.017	0.017	0.235

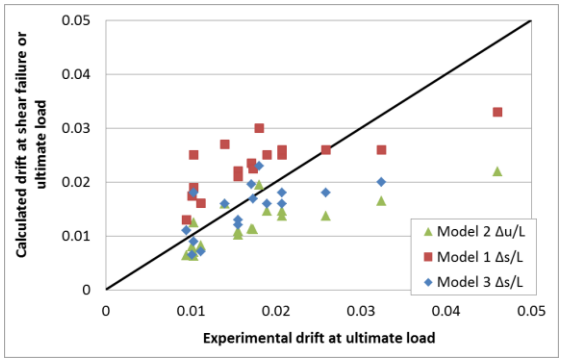

Figure 7: Comparison of drift at ultimate strength or at shear failure

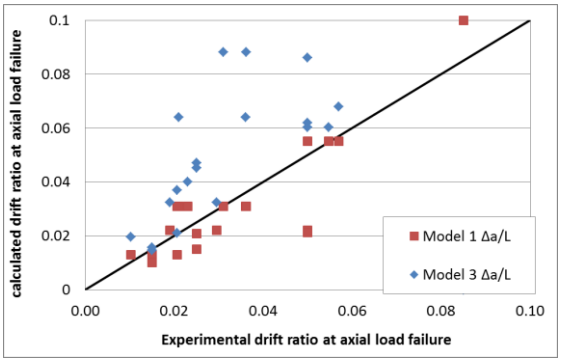

Figure 8: Comparison of drift at axial load failure

4 RESULTS AND DISCUSSION

To examine the validity of the proposed modelling method, simulated results were compared with experimental results for four full-scale columns for which testing was conducted until axial load failure occurred. Details of the columns are provided in Table 3. All of the four columns were reported to exhibit a flexure-shear failure mechanism; however, for Sezen (2002) Spec 2 buckling was also reported. Comparison of the experimental results and the simulated results are shown in Figure 9. The point at which buckling is predicted by Equation (2) is also included to provide an indication of when flexural failure would have been predicted by the model. Furthermore, the points at which yielding and initiation of spalling (i.e. when the concrete strain reaches 0.003) occur are also provided.

It is observed that the simulated results match well with experimental results. The importance of incorporating the shear spring is evident for columns with lower axial loads such as Sezen (2002) Spec 1 and Lynn et al. (1996) 2CLH18, since the sudden strength and stiffness degradation would have not been simulated with the distributed plasticity elements. For columns with higher axial loads such as Sezen (2002) Spec 2 and Lynn et al. (1996) 2CMH18, it can be seen that the drift at which buckling of bars is expected according to Equation (2) approximately corresponds to when instability in the model is observed, as illustrated by the sudden drop in the shear force. The instability in the model is due to the fact that when the deformation limit is reached, the degrading slope of the shear spring is very steep since the drift at shear and axial load failure are similar. In fact for Lynn et al. (1996) 2CMH18 the predicted drift at axial failure is lower than the drift at shear failure, and thus the column suddenly loses its ability to resist lateral and gravity loading (as observed during the experiment as well).

Table 3: Summary of experimental column details

Specimen	ALR	f_c' (MPa)	f_{yl} (MPa)	f_{yt} (MPa)	ρ_l	ρ_t
Sezen (2002) Spec 1	15 %	21.1	438	476	0.025	0.002
Sezen (2002) Spec 2	60 %	21.1	438	476	0.025	0.002
Lynn et al. (1996) 2CLH18	7 %	33.1	331	400	0.019	0.007
Lynn et al. (1996) 2CMH18	28 %	25.5	331	400	0.019	0.007

ALR: Axial load ratio | f_c': concrete characteristic concrete compressive strength | f_{yl}: longitudinal bar yield strength | f_{yt}: transverse bar yield strength | ρ_l: longitudinal bar reinforcement ratio | ρ_t: transverse reinforcement ratio

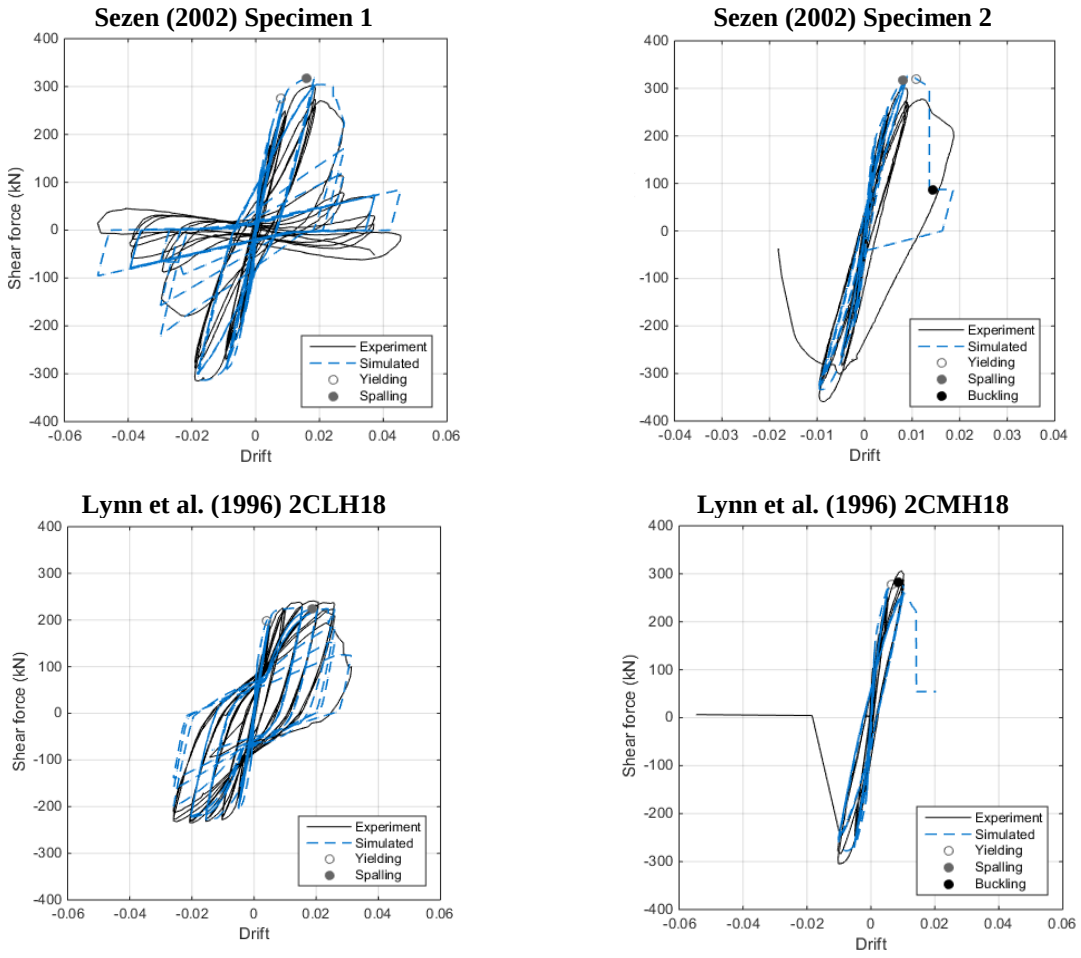

Figure 9: Comparison between simulated and experimental shear force versus drift response of columns (note that buckling strain limit is not reached for Sezen (2002) Spec 1 and Lynn et al. (1996) 2CLH18)

5 CONCLUSION

A brief overview of the current best practice for modelling non-ductile columns has been provided in this paper. An important aspect of modelling columns with low ductility is the incorporation of the shear response, as significant strength and stiffness degradation may follow after the columns have yielded in flexure. The parameters required to define the shear response are challenging and often the empirical based models are limited to the database which they have been based on. This study examined three well established empirically-based models to determine a suitable model to assess the performance of non-ductile columns. The adopted modelling approach in this study is shown to provide a good match with experimental results; however, it is also observed that numerical stability is not easily achieved for columns with high axial loads due to very steep shear stiffness degradation after the deformation limit is reached.

6 REFERENCES

Berry, M. P. (2006). *Performance modeling strategies for modern reinforced concrete bridge columns.* (PhD Dissertation), University of Washington, Seattle, WA.

Dhakal, P., & Maekawa, K. (2002). Reinforcement stability and fracture of cover concrete in reinforced concrete members. *Journal of Structural Engineering, ASCE, 128*(10), 1253-1262.

Elwood, K. J. (2004). Modelling failures in existing reinforced concrete columns. *Canadian Journal of Civil Engineering, 31*(5), 846-859. doi: 10.1139/l04-040

Elwood, K. J., & Moehle, J. P. (2003). Shake table tests and analytical studies on the gravity load collapse of reinforced concrete frames *Pacific Earthquake Engineering Research Center, PEER Report 2003/01*. University of California, Berkeley.

Ghannoum, W. M., & Moehle, J. P. (2012). Dynamic collapse analaysis of a concrete frame sustaining column axial failures. *ACI Structural Journal, 109*(3), 403-412.

Gomes, A., & Appleton, J. (1997). Nonlinear cyclic stress-strain relationship of reinforcing bars including buckling. *Engineering Structures, 19*(10), 822-826.

Ho, J. C. M., & Pam, H. J. (2004). Extent of critical region and limited ductility design of high-strength reinforced concrete columns for Hong Kong practice. *HKIE Transactions, 11*(3), 17-28. doi: 10.1080/1023697X.2004.10667964

LeBorgne, M. R. (2012). *Modeling the post shear failure behaviour of reinforced concrete columns.* (PhD Dissertation), The University of Texas at Austin.

LeBorgne, M. R., & Ghannoum, W. M. (2014). Calibrated analytical element for lateral-strength degradation of reinforced concrete columns. *Engineering Structures, 81*, 35-48. doi: 10.1016/j.engstruct.2014.09.030

Lynn, A. C., Moehle, J. P., Mahin, S. A., & Holmes, W. T. (1996). Seismic evaluation of existing reinforced concrete building columns. *Earthquake Spectra, 12*(4), 715-739.

Mander, J. B., Priestley, M. J. N., & Park, R. (1988). Theoretical stress-strain model for confined concrete. *ASCE Journal of Structural Engineering, 114*(8), 1804-1825.

McKenna, F., Fenves, G. L., Scott, M. N., & Jeremic, B. (2000). Open System for Earthquake Engineering Simulation (OpenSees) (Version 2.4.5, 2013): Pacific Earthquake Engineering Research Center, University of California, Berkeley, CA. Retrieved from http://opensees.berkeley.edu/

Menegotto, M., & Pinto, P. E. (1973). *Method of analysis for cyclically loaded reinforced concrete plane frames including changesin geometry and non-elastic behavior of elements under combined normal force and bending.* Paper presented at the IABSE Sympoium on Resistance and Ultimate Deformability of Structures Acted on by Well-Defined Repeated Loads, International Association for Bridge and Structural Engineering, Zurich, Switzerland.

Moyer, M. J., & Kowalsky, M. J. (2003). Influence of tension strain on buckling of re-bar in concrete columns. *ACI Structural Journal, 100*(1), 75-85.

NZSEE. (2006). Assessment and improvement of the structural performance of buildings in earthquakes *Recommendations of a NZEE study group on earthquake risk buildings June 2006: including corrigendum Nos 1, 2 & 3*: New Zealand Society for Earthquake Engineering.

Popovics, S. (1973). A numerical approach to the complete stress strain curve for concrete. *Cement and concrete research, 3*(5), 583-599.

Saatcioglu, M., & Ozcebe, G. (1989). Response of reinforced concrete columns to simulated seismic loading. *ACI Structural Journal*, 3-12.

Sezen, H. (2002). *Seisic behavior and modeling of reinforced concrete columns.* (PhD Dissertation), University of California, Berkeley.

Stirrat, A. T., Gebreyohaness, A. S., Jury, R. D., & Kam, W. Y. (2014). *Seismic performance assessment of non-ductile columns.* Paper presented at the New Zealand Society Earthquake Engineering (NZSEE) Conference, Auckland, NZ.

Wibowo, A., Wilson, J. L., Lam, N. T. K., & Gad, E. F. (2014). Drift performance of lightly reinforced concrete columns. *Engineering Structures, 59*, 522-535. doi: 10.1016/j.engstruct.2013.11.016

Wilson, J. L., Lam, N. T. K., & Gad, E. F. (2015). *Hazard identification and behaviour of reinforced concrete framed buildings in regions of lower seismicity.* Paper presented at the Tenth Pacific Conference on Earthquake Engineering (PCEE), Building an Earthquake-Resilient Pacific, Sydney, Australia.

Zhao, J., & Sritharan, S. (2007). Modeling of strain penetration effects in fiber-based analysis of reinforced concrete structures. *ACI Structural Journal, 104*(2), 133-141.

APPENDICES

Table A1: Summary of empirical equations for the three models

	Critical parameter	Equation
Model 1	Drift at shear failure	$\frac{\Delta_s}{L} = \frac{3}{100} + 4\rho_t - \frac{1}{40}\frac{v}{\sqrt{f_c'}} - \frac{1}{40}\frac{P}{A_g f_c'} \geq \frac{1}{100}$ Where: $\rho^{"}$ is the transverse reinforcement ratio v is the nominal shear stress (in MPa) f_c' is concrete compressive strength P is the axial load on the column A_g is the column cross-sectional area
	Drift at axial load failure	$\frac{\Delta_a}{L} = \frac{4}{100}\frac{1+(\tan\theta)^2}{\tan\theta + P\left(\frac{s}{A_{st} f_{yt} d_c \tan\theta}\right)}$ Where: d_c is the depth of the column core from centre line to centre line of the ties A_{st} is the area of the transverse reinforcement f_{yt} is the yield strength of the transverse reinforcement θ is the critical crack angle from the horizontal, assumed to be 65°
Model 2	Total rotation limit of hinge region	$\theta_f = 0.027 - 0.033\frac{P}{A_g f_c'} - \frac{0.01s}{d} \geq 0.006$ Where: P is the axial load on the column A_g is the column cross-sectional area f_c' is concrete compressive strength s is the spacing of the ties d is the effective depth of the column
	Residual drift ratio of the shear spring	$\frac{\Delta_r}{L} = 0.16 - 15.4\rho_t - 0.009\frac{l_d}{d_b} + \frac{0.7A_{cc}}{A_g} + 0.58\frac{f_y A_s}{f_c' A_g} \geq 0.02$ Where: L is the clear length of the column ρ_t is the transverse reinforcement ratio l_d is the development length of the longitudinal bars as given by ACI A_g is the gross column cross-section A_{cc} is the confined area of the column cross-section A_s total area of the longitudinal bars f_y is the yield strength of the longitudinal bars
Model 3	Drift at ultimate shear force	$\frac{\Delta_u}{L} = \frac{\Delta_y}{L} + \frac{\Delta_p}{L}$ Where: $\Delta_y = \frac{\phi_y L^2}{3}$ for cantilever columns, where ϕ_y is thee curvature from sectional analysis $\frac{\Delta_p}{L} = (\phi_u - \phi_y)L_p$, where L_p is plastic hinge length $L_p = 0.5D$, D is the column depth ϕ_u is the ultimate curvature from sectional analysis
	Drift at axial load failure (when shear resistance drops below 50% of the peak strength)	$\frac{\Delta_a}{L} = 5(1+\rho_v)^{-\frac{1}{1-\beta}} + 7\rho_h + \frac{1}{5n}$ Where ρ_v is the longitudinal reinforcement ratio $\rho_h$is the transverse reinforcement ratio $\beta = \frac{n}{n_b}$, where n is the axial load ratio, and n_b is the axial load ratio at the balance point on the interaction diagram
	Drift at shear failure	Calculated using linear interpolation between $\frac{\Delta_u}{L}$ and $\frac{\Delta_a}{L}$.

Table A2: Detail of columns included in the database in this study

Specimen	ALR	f_c' (MPa)	f_{yl} (MPa)	f_{yt} (MPa)	ρ_l	ρ_t	a
Sezen (2002) Spec 1	15.0%	21.1	438	476	0.025	0.002	3.2
Sezen (2002) Spec 2	60.0%	21.1	438	476	0.025	0.002	3.2
Sezen (2002) Spec 3	60.0%	20.9	438	476	0.025	0.002	3.2
Sezen (2002) Spec 4	15.0%	21.8	438	476	0.025	0.002	3.2
Lynn et al. (1996) 3CLH18	9.4%	25.6	331	400	0.03	0.0007	3.2
Lynn et al. (1996) 2CLH18	7.3%	33.1	331	400	0.019	0.0007	3.2
Lynn et al. (1996) 3SLH18	9.4%	25.6	331	400	0.03	0.0007	3.2
Lynn et al. (1996) 2SLH18	7.3%	33.1	331	400	0.019	0.0007	3.2
Lynn et al. (1996) 2CMH18	28.4%	25.5	331	400	0.019	0.0007	3.2
Lynn et al. (1996) 3CMH18	26.2%	27.6	331	400	0.03	0.0007	3.2
Lynn et al. (1996) 3CMD12	26.2%	27.6	331	400	0.03	0.0020	3.2
Lynn et al. (1996) 3SMD12	28.4%	25.5	331	400	0.03	0.0020	3.2
Ho and Pam (2004) 1A	13.0%	70.0	531	357	0.0086	0.0018	4.66
Ho and Pam (2004) 2A	33.0%	80.0	522	357	0.024	0.0031	4.66
Fardipour (2012) Spec 1	20.0%	20.3	527	365	0.0056	0.0007	4
Fardipour (2012) Spec 2	20.0%	21.0	515	365	0.01	0.0007	4
Fardipour (2012) Spec 3	40.0%	18.4	515	365	0.01	0.0007	4
Fardipour (2012) Spec 4	40.0%	24.2	527	365	0.0056	0.0007	4
Saatcioglu and Ozcebe (1989) U1	0%	43.6	430	470	0.032	0.0030	2.86
Saatcioglu and Ozcebe (1989) U2	16.0%	30.2	453	470	0.032	0.0030	2.86

ALR: Axial load ratio | f_c': concrete characteristic concrete compressive strength | f_{yl}: longitudinal bar yield strength | f_{yt}: transverse bar yield strength | ρ_l: longitudinal bar reinforcement ratio | ρ_t: transverse reinforcement ratio | a: shear span to column depth ratio